

Study of the Solar Anisotropy for Cosmic Ray Primaries of about 200 GeV Energy with the L3+C Muon Detector

The L3 Collaboration

Abstract

Primary cosmic rays experience multiple deflections in the non-uniform galactic and heliospheric magnetic fields which may generate anisotropies. A study of anisotropies in the energy range between 100 and 500 GeV is performed. This energy range is not yet well explored. The L3 detector at the CERN electron-positron collider, LEP, is used for a study of the angular distribution of atmospheric muons with energies above 20 GeV. This distribution is used to investigate the isotropy of the time-dependent intensity of the primary cosmic-ray flux with a Fourier analysis. A small deviation from isotropy at energies around 200 GeV is observed for the second harmonics at the solar frequency. No sidereal anisotropy is found at a level above 10^{-4} . The measurements have been performed in the years 1999 and 2000.

To be submitted to Astronomy and Astrophysics

1 Introduction

Cosmic rays of GeV–TeV–PeV energies are galactic in nature and very probably produced mainly by the shocks generated by supernova explosions. Some of these particles reach the Solar System after experiencing multiple deflections in the non-uniform galactic magnetic field, particularly in the neighborhood of the Sun. This generates a structure [1] in the arrival direction of the particles, and the variation of the intensity of primary cosmic rays as a function of the equatorial coordinates α (right ascension) and δ (declination) is well-known as the *sidereal anisotropy*. Thus a detector located on the Earth surface observes a modulation of the cosmic-ray flux with a period of one sidereal day due to the Earth rotation. The magnetic field within the heliosphere, whose structure is strongly influenced by the solar wind and the Sun activity, plays a role in the propagation of galactic cosmic rays with energies of the order of 10 TeV and below. At these energies, the general large-scale structure of the heliomagnetic field may induce structures in the sidereal anisotropy. At lower energies structures may be due mainly to the Solar wind plasma. Additional cosmic-ray intensity variations may depend on the arrival direction with respect to Sun. These would appear as an intensity modulation with a period of one Solar day, known commonly as the *solar anisotropy*. In addition, the orbital motion of the Earth is expected to produce a signal modulated with this frequency. This effect, called the Compton-Getting effect, is well understood and can be corrected for [2]. Possible observations of a modulation in the cosmic-ray flux should be carefully analysed to account for changes in the muon production rate and energy loss in the atmosphere due to meteorological effects, such as diurnal and seasonal variations of temperature and pressure.

The presently available data on the anisotropy may be summarized as follows. Except for the very recent observation of an anisotropy on the most energetic cosmic-rays above 60 EeV by the AUGER collaboration [3], no anisotropy at primary energies above 300 TeV has been observed [4, 5]. No effect due to the heliosphere, nor to the galactic Compton-Getting effect due to the solar system orbiting around the center of the galaxy, has been detected. For primary energies between 4 and 50 TeV a clear sidereal anisotropy is present [5]. The GRAND collaboration observed a very significant solar anisotropy, expressed as the sum of the first two harmonics, around 10 GeV [6].

The energy range for primaries between 100 and 500 GeV has not yet been fully explored. This is the domain the L3+C detector is sensitive to, and the subject of this analysis. The anisotropy of primary cosmic rays is studied indirectly through the observation of muons which result from the

decay of the secondary particles produced in the Earth atmosphere. The median primary energy corresponding to a given muon energy threshold is about 10 times larger than the muon energies [7]. For a muon energy above 20 GeV the muon direction approximates, within 3° , the direction of the primary [8].

The analysis of the experimental data for studies on anisotropy is based on the expansion in spherical harmonics of the anisotropy function, defined as [9]

$$\Delta^{dir}(\alpha, \delta) = \frac{I(\alpha, \delta) - \langle I \rangle}{\langle I \rangle} \quad (1)$$

where $I(\alpha, \delta)$ is the intensity as a function of the right ascension α and declination δ and $\langle I \rangle$ is the mean intensity.

Anisotropy measurements at a level of 10^{-4} and better can be achieved by scanning a band with fixed declination range in the right ascension direction [10]¹⁾. In this analysis the anisotropy function is reduced to a quantity independent of the declination, and is defined for the particular declination distribution given by the L3+C direction-dependent acceptance. Information about the anisotropy on large scales is estimated from the first few terms of the Fourier expansion of $\Delta(\alpha)$:

$$\Delta(\alpha) = \sum_{m=1}^{\infty} \xi_m \cos(m(\alpha - \phi_m)) \quad (2)$$

where ξ_m and ϕ_m are the corresponding amplitudes and phases of the m -th harmonics respectively.

2 The L3+C detector and the event selection

The L3 detector [14] operated at the LEP accelerator at CERN (nearby Geneva, Switzerland). It was located 30 m under ground, at 450 m above sea level, at a longitude of 6.02° E and a latitude of 46.25° N. It was designed to measure accurately muons, electrons and photons produced in e^+e^- collisions. The momentum distribution of atmospheric muons is measured with an upgraded setup known as L3+C [15]. The parts of the detector used in this analysis are sketched in Figure 1.

After passing through the stratified rock overburden, called "molasse" (sedimentary rocks), the arrival time t_0 of a muon is measured with a resolution of 1.7 ns by a 202 m² scintillator array placed on top of the detector. The

¹⁾The Tibet, Super-Kamiokande, and MILAGRO collaborations have recently performed two-dimensional measurements for primary energies above a few TeV [5, 11–13].

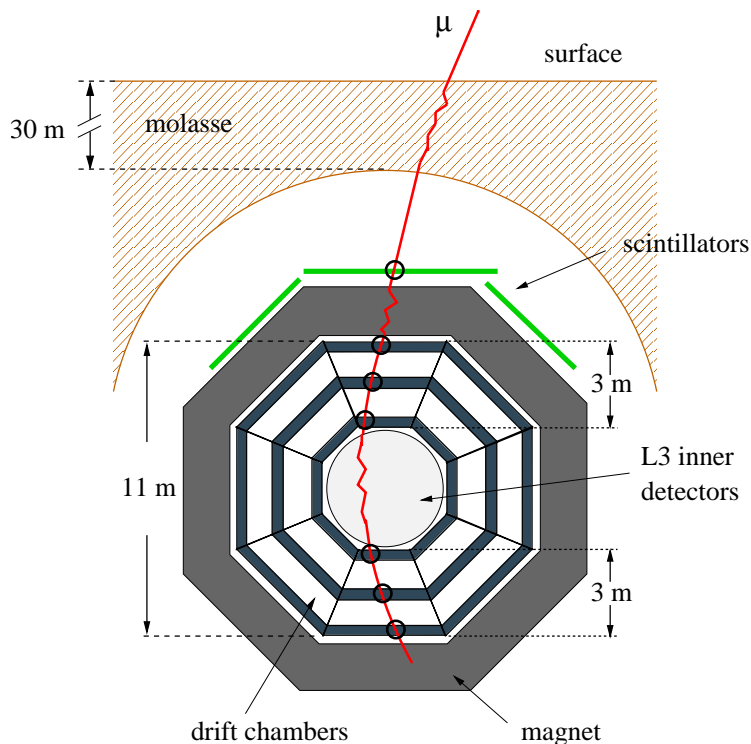


Figure 1: Schematic view of the experimental setup.

array is composed of 34 modules, each read out by two photomultipliers in coincidence to reduce noise. Inside a volume of about 1000 m^3 , with a magnetic field of 0.5 T, the coordinates and slopes of a muon track are measured in up to six drift chambers in the bending plane and up to eight times in the non-bending plane. These chambers are arranged concentrically around the LEP beam in line on two ferris wheels of eight octants, each containing three layers of drift cells. By subtracting the t_0 time from the arrival times of the drift electrons at the sense wires, a track position in each chamber can be reconstructed with a precision of about $60 \mu\text{m}$ in the bending plane and 1 mm in the non-bending plane.

Only three points are needed to determine the radius of the track in the magnetic field, therefore the momentum of a muon traversing two octants can be measured twice. This redundancy is used to evaluate the detector efficiencies and the resolution of the apparatus. The best resolution is obtained when fitting the six points together over the full track length of 11 meters. The multiple scattering and energy loss inside the L3 inner detectors, as well as the effect of the inhomogeneous magnetic field are taken into account in the

event reconstruction [16]. For vertically incident muons, the mean energy loss in the molasse and the magnet is 19 GeV at low momenta and reaches 57 GeV at 1 TeV.

The detector achieved excellent muon momentum resolutions, 4.6 % at 45 GeV and an angular resolution of better than 0.3° at 100 GeV [17, 18].

L3+C recorded 1.2×10^{10} muon triggers during its operation from mid July to November 1999 and April to November 2000.

This analysis is restricted to events which satisfy two criteria: muon tracks must be reconstructed from at least three chambers in any octant and a hit in the scintillators; exactly one track must be successfully reconstructed as coming from the surface. A selection of the time intervals of data taking is applied in order to assure stability in the detection efficiency. To account for muon rate variations due to meteorological effects and efficiency fluctuations a running average of the detection rate is calculated for every selected run over an interval of time lasting 12 hours before the run to 12 hours after the run. When filling the histogram corresponding to the live-time distribution, the contents are weighted with a factor proportional to this running average [19, 20]. The Compton-Getting effect is taken care of by applying a weight factor to each event, according to the muon arrival direction and the Earth orbital velocity.

The analysed data correspond to a total live-time of 150.63 days, evenly distributed over the full data taking period. Muon samples were selected according to four different lower energy cuts in order to detect a possible energy dependence of the anisotropy: 20, 30, 50 and 100 GeV.

3 Data analysis

The anisotropy of primary cosmic rays is studied based on the idea that a fixed detector scans the sky in the right ascension direction (α), thanks to the Earth rotation. Figure 2 shows distributions in declination of the events selected for four muon energy thresholds. The detector acceptance is energy dependent because of different material thicknesses crossed by the muons. For example, the structure observed for the lowest energy threshold around 55° is caused by the access shaft to the detector underground cavern.

The analysis method searches for time variations of the muon detection rates with a period of one day, regardless of the arrival direction of the muons.

This study introduces a method that takes into account the directional information, α , available from the reconstruction of the muon tracks [10]. For the sidereal anisotropy, the expected distribution $N_\mu^{\text{exp}}(\alpha)$ of muon events as a

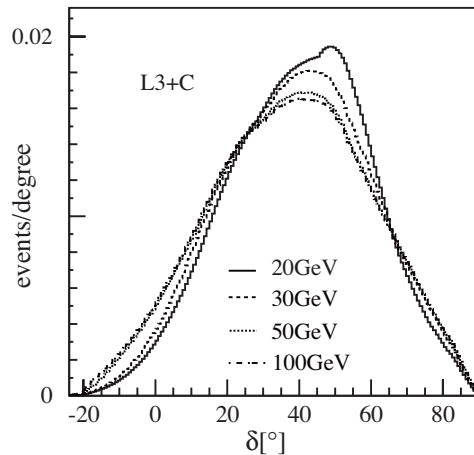


Figure 2: Distributions of the analyzed events as a function of the declination δ for different lower energy cuts. The distributions are normalized to 1.

function of α in the case of an isotropic primary cosmic ray flux is calculated by folding the observed event distribution as a function of the negative hour angle, $-h.a.$, with the live-time distribution of the sidereal time t_s . Typical distributions of these two quantities are shown in Figure 3. $N_\mu^{\text{exp}}(\alpha)$ is then compared with the actual measured distribution $N_\mu^{\text{meas}}(\alpha)$ and $\Delta(\alpha)$ is calculated as:

$$\Delta(\alpha) = \frac{N_\mu^{\text{meas}}(\alpha)}{N_\mu^{\text{exp}}(\alpha)} - 1. \quad (3)$$

Figure 4 compares the measured event distribution with the expected distribution for muons above 30 GeV. As an example, only data for one day are displayed. On such time scale the statistical fluctuations of the measured distribution around the smooth curve of the expected distribution are visible. Figure 5 represents the corresponding result of equation (3).

A harmonic analysis of the result is performed to extract the first three harmonics of $\Delta(\alpha)$ at the sidereal frequency.

If frequencies ν , other than the sidereal frequency ν_* , are considered, then the pseudo-right ascension $\tilde{\alpha}_\nu$ is used instead of α . It is defined as

$$\tilde{\alpha}_\nu = [\phi_\nu - h.a.]_{\text{mod}24\text{h}} \quad (4)$$

where the phase ϕ_ν is defined as

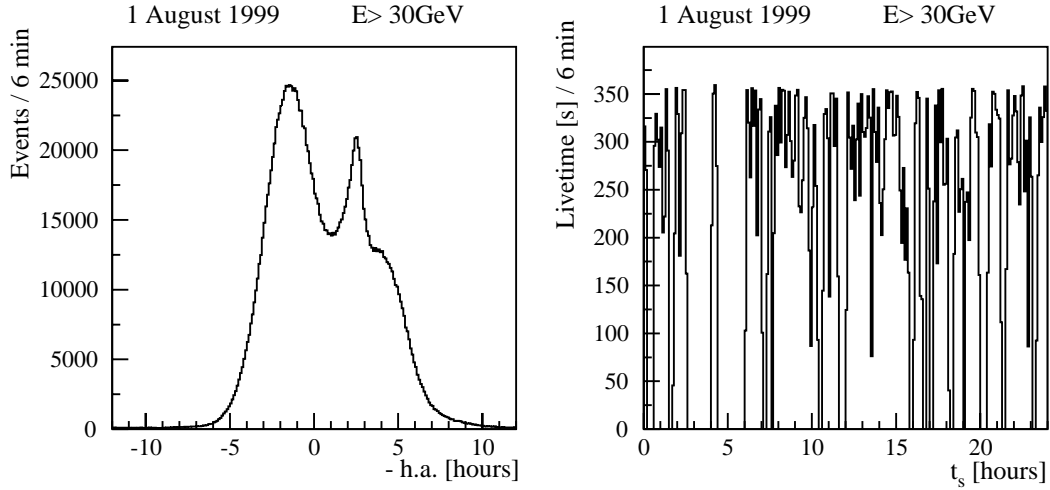


Figure 3: Distributions of the event negative hour angle and (right-hand side) livetime for muons with a surface energy above 30 GeV obtained from data acquired during one day (1st of August 1999). The selection of good-quality data taking conditions is responsible for the live-time fluctuations. The convolution of the two distributions gives the expected distribution, under the assumption of isotropy.

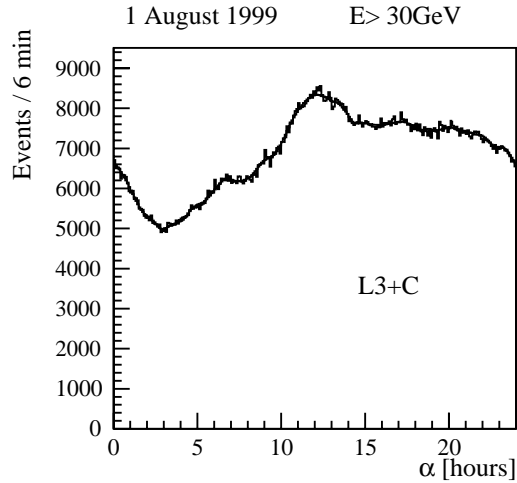


Figure 4: Measured (binned data) and expected (black line) event distribution in right ascension for muons with a surface energy larger than 30 GeV detected during one day (1st of August 1999). The structures are due to the live-time distribution presented in Figure 3.

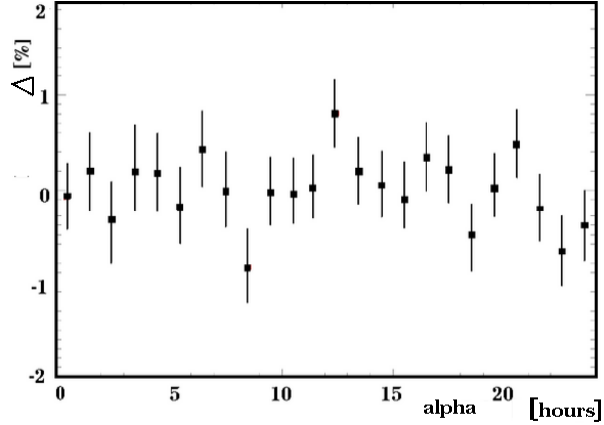


Figure 5: The computed ratio between the two distributions shown in Figure 4, according to equation (3).

$$\phi_\nu = \frac{\nu}{\nu_\odot}(t - t_0) + t_l \quad (5)$$

and where ν_\odot is the solar frequency (1/24 hours), t is the time of the observation, t_0 is a conventional time point which defines when $\tilde{\alpha}_\nu$ is equal for all frequencies and t_l is a free phase shift parameter.

We choose t_0 to be the time near the autumn equinox when in the year 2000 the mean local solar time and the local sidereal time are the same and are equal to t_l . Thus for the solar frequency, the Sun is always located approximately at $\tilde{\alpha}_{\nu_\odot} = 12$ hours. In addition to the solar frequency ν_\odot , three other frequencies are interesting: the sidereal frequency ν_* ; the anti-sidereal frequency, which is a side lobe of the same size at the sidereal frequency if a real effect at the solar frequency is modulated with an annual frequency; and the extended sidereal frequency. Other 86 frequencies are analysed for the purpose to check the uncertainties of the measurement. The combined statistical and systematic uncertainties are obtained by considering the distribution of the amplitudes ξ of the 86 frequencies, which should obey the Rayleigh distribution R normalized to 1:

$$R(\xi, \sigma) = \frac{1}{\sigma^2} \xi e^{-\frac{\xi^2}{2\sigma^2}} . \quad (6)$$

The data are fitted to this function for the first three harmonics, and the four energy thresholds. The fitted value of σ is compared to the

expected statistical uncertainty and good agreement is found, leading to the conclusion that systematic uncertainties are negligible compared to the statistical uncertainty.

The amplitude distributions for all 86 frequencies are displayed in Figures 6, and 7 for the 1st and 2nd harmonics.

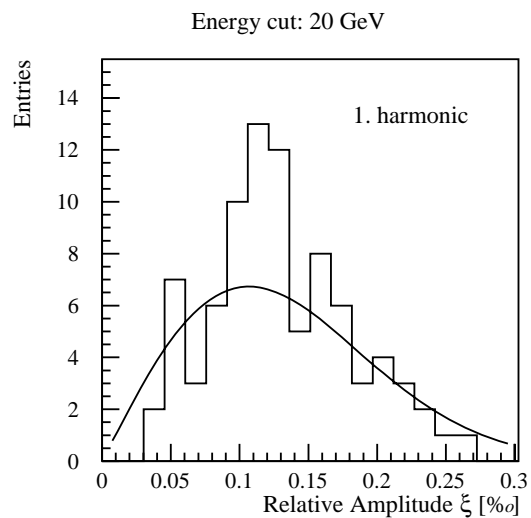


Figure 6: Histogram showing the amplitude distribution ξ_m for the 86 frequencies of the spectrum presented in Figure 9, after excluding the 4 physically interesting ones. The histogram is fitted with the Raleigh distribution ($\chi^2/ndf = 13.7/14$).

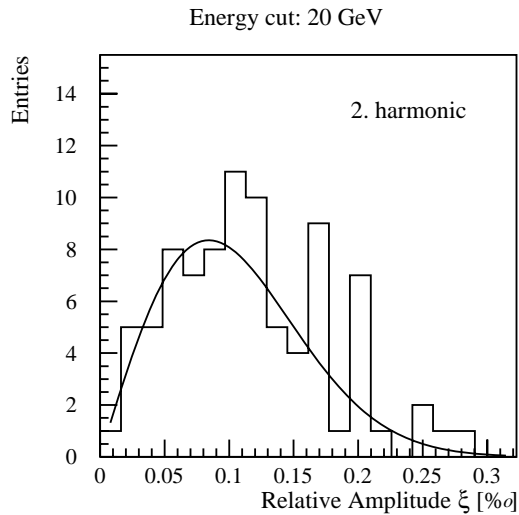


Figure 7: Histogram showing the amplitude distribution ξ_m for the 86 frequencies of the spectrum presented in Figure 10, after excluding the 4 physically interesting ones. The histogram is fitted with the Raleigh distribution ($\chi^2/ndf = 15.01/15$).

4 Results

No significant anisotropy is observed at the sidereal frequency for any of the first three harmonics. Figure 8 presents the case for the first harmonic. The results obtained with a muon energy cut at 100 GeV corresponding to primary protons of 1 TeV are compatible with the experimental result of Cutler and Groom [19], derived from muon data collected from 1978 to 1983 with a threshold of 100 GeV.

For a 200 GeV primary energy threshold, the observation of the first harmonic does not follow the “tail-in” and “loss-cone” model, NFJ, by Nagashima, Fujimoto and Jacklyn [21], which predicts a deficit of galactic origin at $\alpha = 12h$, the so called heliospheric effect. The GRAPES experiment, with a primary energy threshold of 60 GeV, has collected data between 2000 and 2004, at the end of the period where the magnetic field of the sun has changed its polarity and which followed our own data acquisition period. This collaboration observed the NFJ effect only partly, detecting only the “tail-in” part [22].

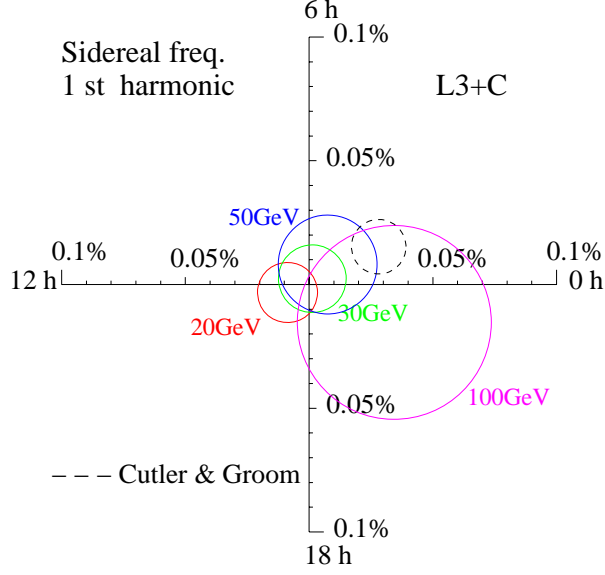


Figure 8: Dial plots showing the amplitude and the phase of the first harmonic of the anisotropy function at the sidereal frequency for four different energy cuts. The axis correspond to the right ascensions 0h, 6h, 12h, and 18h, the radii to the amplitudes whose graduation can be read on the axis. The circles represent the 68.5% confidence level regions for the 4 muon momentum thresholds. The dashed circle is the result of Cutler and Groom [19].

Figures 9 and 10 show the amplitude ξ_m as a function of the frequency for the first and the second harmonic respectively. The muon energy-threshold is set to 20 GeV. The largest amplitude is found for the second harmonic at the solar frequency.

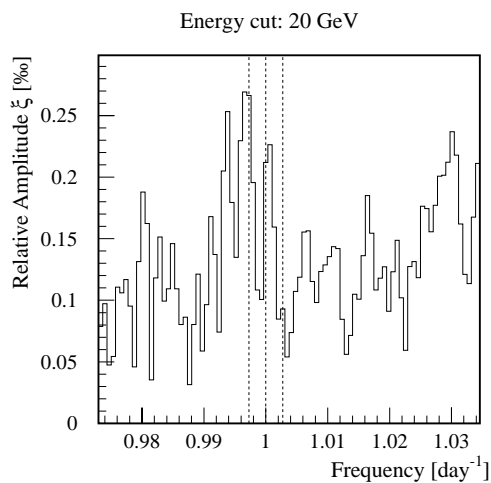


Figure 9: Amplitude ξ_m for the first harmonic of the relative muon intensity variation as a function of $\tilde{\alpha}$ for frequencies near 1 day^{-1} and for a surface energy threshold of 20 GeV. Vertical lines indicate from left to right the anti-sidereal, the solar and the sidereal frequency.

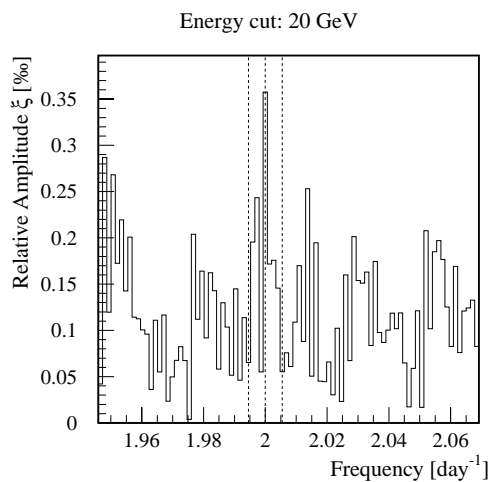


Figure 10: Amplitude ξ_m for the second harmonic of the relative muon intensity variation as a function of $\tilde{\alpha}$ for frequencies near 2 day^{-1} and for a surface energy threshold of 20 GeV. Vertical lines indicate from left to right the double anti-sidereal, the double solar and the double sidereal frequency.

Figure 11 presents the energy dependence. An anisotropy is observed for a muon energy-threshold up to 50 GeV, corresponding to primaries up to 500 GeV. The largest significance is observed for a muon energy-threshold of 20 GeV, where the amplitude is 4.5σ away from 0. In a Rayleigh distribution the probability to find an amplitude larger than that is only $4 \cdot 10^{-5}$.

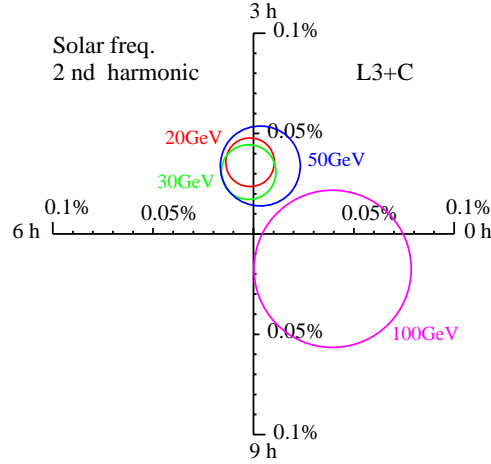


Figure 11: Dial plots showing the amplitude and the phase of the second harmonic of the anisotropy function at the Solar frequency for four different muon energy-cuts. The circles represent the 68.5 % confidence level region.

Figure 12 presents this anisotropy for a muon energy-threshold of 20 GeV. The χ^2 of the fit amounts to 6.6 for 7 degrees of freedom (ndf). (A flat distribution provides a χ^2 equal to 28.3 for $\text{ndf} = 11$. In this case the probability to find a value larger or equal to 28.3 is $2.9 \cdot 10^{-3}$.)

The fact that for the first three energy thresholds the phase is different from the one at 100 GeV is also an interesting feature, in the sense, that it indicates (although with a small significance) an energy dependence of the anisotropy. But as discussed above and by inspecting Figure 11, a real significance is for a muon energy-threshold of 20, and eventually 30 GeV. At 50 and 100 GeV the uncertainties are too large to conclude.

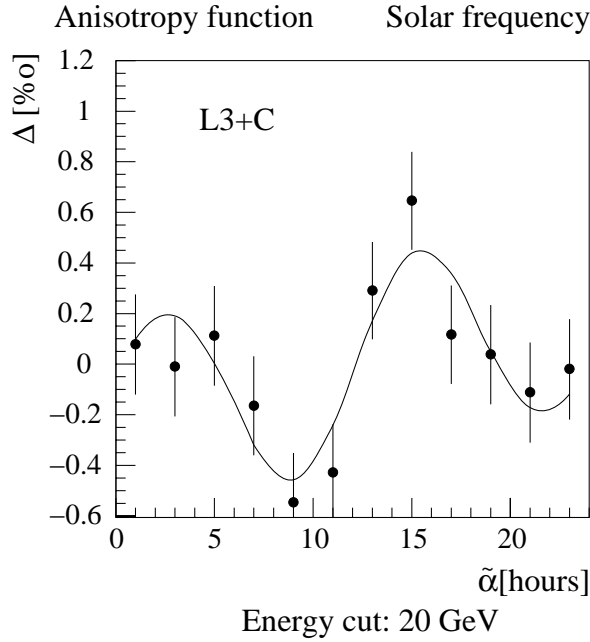


Figure 12: Anisotropy distribution Δ [ρ_{00}] in pseudo-right ascension, $\tilde{\alpha}$, for muons with energy larger than 20 GeV. The continuous line represents the fit to the data with the sum of the first two harmonics ($\chi^2 = 6.6 / 7$ n.d.f.). The vertical bars represent the statistical uncertainties; the systematic uncertainties are negligible.

The structure of the anisotropy function for the 2nd harmonic found is very similar in shape, but five times smaller in amplitude, to what has been reported by the GRAND experiment. This experiment measured the sum of the 1st and 2nd harmonic and was located at 41.7° N and 86.2° W. It had a 0.1 GeV muon threshold energy and collected data between 1997 and 2000 [6]. The observed diurnal peak in solar time has been explained according to Hall, Duldig and Humble [23] with the fact that cosmic rays are partially affected by the solar wind.

For muon energies above 100 GeV the effect was reported in 2003 by the MACRO collaboration [24, 25].

No anisotropy is found from the analysis of the 3rd harmonic for any of the four muon threshold-energy.

A summary of the results of the spectral analysis for the solar frequency is given in Table 1.

The analyses of multi-muon events with multiplicities larger than 3, compared to the single muon events discussed above, show no significant deviation from isotropy. This result can be compared to earlier studies claiming

an increase of the anisotropy for heavy primaries, producing higher muon multiplicities [26].

Energy cut [GeV]	m-th harmonic	ξ_m [per mil]	ϕ_m [hr]	ρ_{error} [per mil]	σ_{stat} [per mil]
20	1st	0.21	18.2	0.12	0.08
	2nd	0.36	3.1		
	3rd	0.18	6.9		
30	1st	0.16	20.7	0.14	0.09
	2nd	0.31	3.2		
	3rd	0.13	7.2		
50	1st	0.10	2.9	0.20	0.13
	2nd	0.34	2.8		
	3rd	0.15	7.6		
100	1st	0.28	22.0	0.40	0.26
	2nd	0.43	11.2		
	3rd	0.36	7.5		

Table 1: Amplitudes, ξ_m , and phases, ϕ_m , of the first three harmonics obtained from the spectral analysis of the anisotropy function for the solar frequency for different muon energy thresholds. $\rho_{error} = 1.52 \sigma_{stat}$ is the radius of the error circle defining a 68.5% confidence level region. The uncertainties are statistical.

5 Conclusions

Indirect measurements of the anisotropy of primary cosmic rays with energies around 200 GeV do not show any sidereal anisotropy at a level above 10^{-4} . The largest deviation from isotropy is found for the second harmonics at solar frequency for muons above an energy threshold of 20 GeV, corresponding to primaries with energies of about 200 GeV. The amplitude is 4.5σ away from 0. In explaining this effect, e.g. as a manifestation of the interaction of cosmic rays with the Solar wind plasma, one has to take into account the complexity and variability of the solar magnetic field during the time of data collection that occurred near the maximum of solar activity. In addition one should consider that the effect is certainly energy dependent, and that uncertainties exist about the magnetic field in the neighbourhood of the Sun.

Acknowledgments

The L3 collaboration would like to thank CERN for the support given to this experiment, and express in particular its gratitude to the crew operating at LEP point 2 for the successful installation of the additional hardware needed for L3+C.

References

- [1] M. Amenomori *et al.*, *Ap. J. Letters* **626** (2005) L29;
A.D. Erlykin and A.W. Wolfendale, *Astropart. Phys.* **25** (2006) 183.
- [2] A.H. Compton and I.A. Getting, *Phys. Rev.* **47** (1935) 817.
- [3] AUGER collab., J. Abraham *et al.*, *Science* **318** (2007) 938.
- [4] G. Maier *et al.*, in Proc. of the XVIIIth ICRC, Tsukuba 2003, p.179.
- [5] M. Amenomori *et al.*, *Science* **314** (2006) 439.
- [6] J. Poirier *et al.*, in Proc. of the XVII th ICRC, Hamburg, 2001, p. 3934;
J. Poirier, C. D’Andrea, and M. Dunford, astro-ph/0109462.
- [7] T.K. Gaisser, “Cosmic Rays and Particle Physics”, Cambridge University Press, 1990, p. 73.
- [8] D. Heck, D. *et al.*, CORSIKA - Technical report, FZKA 6019, Forschungszentrum Karlsruhe (1998).
- [9] P. Király *et al.*, *Rivista del Nuovo Cimento* **2 Vol.7** (1979) 1.
- [10] R. Ramelli, “Search for Cosmic Ray Point Sources and Anisotropy Measurement with the L3+C Experiment”, Ph.D. thesis No. 14683, ETH-Zürich, 2002.
L3 collab., P. Achard *et al.*, *Astropart. Phys.* **25** (2006) 298.
- [11] Super-Kamiokande collab., G. Guillian *et al.*, *Phys. Rev. D* **75** (2007) 062003.
- [12] R. Atkins *et al.*, *Phys. Rev. Lett.* **95** (2005) 251103.
- [13] G.G. McGrath, “A Treatise on High Energy Muons in the IMB Detector”, Ph.D. thesis, University of Hawaii, Manoa (1993).

- [14] L3 detector, B. Adeva *et al.*, *Nucl. Instr. Meth.* **A 289** (1990) 35.
- [15] O. Adriani *et al.*, *Nucl. Instr. Meth.* **A 488** (2002) 209.
- [16] V. Innocente and E. Nagy, *Nucl. Instr. Meth.* **A 324** (1993) 297.
- [17] L3 collab., P. Achard *et al.*, *Phys. Lett.* **B 598** (2004) 15.
- [18] L3 collab., P. Achard *et al.*, *Astropart. Phys.* **23** (2005) 411.
- [19] D.J. Cutler and D.E. Groom, *Astrophys. J.* **376** (1991) 322, *ibid.* **248** (1981) 2266.
- [20] S.K. Gerasimova *et al.*, in Proc. of the XVIIth ICRC, Hamburg 2001, p. 3959.
- [21] K. Nagashima, K. Fujimoto, and R.M. Jacklyn, *J. Geophys. Res.* **103** (1998) 17429.
- [22] GRAPES collab., H. Kojima *et al.*, in Proc. of the XXIX th ICRC, Pune, 2005, Vol. 2, p. 81.
- [23] D.L. Hall, M.L. Duldig, and J.E. Humble, *Space Science Reviews* **78** (1996) 401; and in *Astrophys. J.* **482** (1997) 1083.
- [24] MACRO collab., M. Ambrosio, *et al. Phys.Rev.* **D 67** (2003) 042002.
- [25] MACRO collab., Y. Becherini, *et al.*, in Proc. of the XXIX th ICRC, Pune, 2005, Vol. 6, p. 157;
Y. Becherini *et al.*, astro-ph/0510187.
- [26] G. Bressi *et al.*, *Europhys. Lett.* **11** (1990) 287.

The L3 Collaboration:

P.Achard,²² O.Adriani,¹⁹ M.Aguilar-Benitez,²⁷ M.van den Akker,³³ J.Alcaraz,²⁷ G.Alemanni,²⁵ J.Allaby,²⁰ A.Aloisio,³¹ M.G.Alvigi,³¹ H.Anderhub,⁵³ V.P.Andreev,^{6,37} F.Anselmo,¹⁰ A.Arefiev,³⁰ T.Azmoon,³ T.Aziz,¹¹ P.Bagnaia,⁴² A.Bajo,²⁷ G.Baksay,²⁸ L.Baksay,²⁸ J.Bähr,⁵² S.V.Baldew,² S.Banerjee,¹¹ Sw.Banerjee,⁴ A.Barczyk,^{53,51} R.Barillère,²⁰ P.Bartalini,²⁵ M.Basile,¹⁰ N.Batalova,⁵⁰ R.Battiston,³⁶ A.Bay,²⁵ F.Becattini,¹⁹ U.Becker,¹⁵ F.Behner,⁵³ L.Bellucci,¹⁹ R.Berbeco,³ J.Berdugo,²⁷ P.Berges,¹⁵ B.Bertucci,³⁶ B.L.Betev,⁵³ M.Biasini,³⁶ M.Biglietti,³¹ A.Biland,⁵³ J.J.Blaising,⁴ S.C.Blyth,³⁸ G.J.Bobbink,² A.Böhm,¹ L.Boldizsar,¹⁴ B.Borgia,⁴² S.Bottai,¹⁹ D.Bourilkov,⁵³ M.Bourquin,²² S.Braccini,²² J.G.Branson,⁴⁴ F.Brochu,⁴ J.D.Burger,¹⁵ W.J.Burger,³⁶ X.D.Cai,¹⁵ M.Capell,¹⁵ G.Cara Romeo,¹⁰ G.Carlino,³¹ A.Cartacci,¹⁹ J.Casaus,²⁷ F.Cavallari,⁴² N.Cavallo,³⁹ C.Cecchi,³⁶ M.Cerrada,²⁷ M.Chamizo,²² Y.H.Chang,⁴⁸ M.Chemarin,²⁶ A.Chen,⁴⁸ G.Chen,⁷ G.M.Chen,⁷ H.F.Chen,²⁴ H.S.Chen,⁷ T.Chiarusi,¹⁹ G.Chiefari,³¹ L.Cifarelli,⁴³ F.Cindolo,¹⁰ I.Clare,¹⁵ R.Clare,⁴¹ G.Coignet,⁴ N.Colino,²⁷ S.Costantini,⁴² B.de la Cruz,²⁷ S.Cucciarelli,³⁶ R.de Asmundis,³¹ P.Déglon,²² J.Debreczeni,¹⁴ A.Degré,⁴ K.Dehmelt,²⁸ K.Deiters,⁵¹ D.della Volpe,³¹ E.Delmeire,²² P.Denes,⁴⁰ F.DeNotaristefani,⁴² A.De Salvo,⁵³ M.Diemoz,⁴² M.Dierckxsens,² L.K.Ding,⁷ C.Dionisi,⁴² M.Dittmar,⁵³ A.Doria,³¹ M.T.Dova,^{12,‡} D.Duchesneau,⁴ M.Duda,¹ I.Duran,⁴⁵ B.Echenard,²² A.Eline,²⁰ H.El Mamouni,²⁶ A.Engler,³⁸ F.J.Eppling,¹⁵ P.Extermann,²² G.Faber,⁵³ M.A.Falagan,²⁷ S.Falciano,⁴² A.Favara,³⁵ J.Fay,²⁶ O.Fedin,³⁷ M.Felcini,⁵³ T.Ferguson,³⁸ E.Fiandrini,³⁶ J.H.Field,²² F.Filthaut,³³ W.Fisher,⁴⁰ G.Forconi,¹⁵ K.Freudenreich,⁵³ C.Furetta,²⁹ Yu.Galaktionov,^{30,15} S.N.Ganguli,¹¹ P.Garcia-Abia,²⁷ M.Gataullin,³⁵ S.Gentile,⁴² S.Giagu,⁴² Z.F.Gong,²⁴ H.J.Grabosch,⁵² G.Grenier,²⁶ O.Grimm,⁵³ H.Groenstege,² M.W.Gruenewald,¹⁸ Y.N.Guo,⁷ S.Gupta,¹¹ V.K.Gupta,⁴⁰ A.Gurtu,¹¹ L.J.Gutay,⁵⁰ D.Haas,⁵ Ch.Haller,⁵³ D.Hatzifotiadou,¹⁰ Y.Hayashi,³⁴ Z.X.He,⁸ T.Hebbeker,¹ A.Hervé,²⁰ J.Hirschfelder,³⁸ H.Hofer,⁵³ H.Hofer,jun.,⁵³ M.Hohlmann,²⁸ G.Holzner,⁵³ S.R.Hou,⁴⁸ A.X.Huo,⁷ N.Ito,³⁴ B.N.Jin,⁷ P.Jindal,¹⁶ C.L.Jing,⁷ L.W.Jones,³ P.de Jong,² I.Josa-Mutuberría,²⁷ V.Kantserov,^{52,⊙} M.Kaur,¹⁶ S.Kawakami,³⁴ M.N.Kienzle-Focacci,²² J.K.Kim,⁴⁷ J.Kirkby,²⁰ W.Kittel,³³ A.Klimentov,^{15,30} A.C.König,³³ E.Kok,² A.Korn,¹⁵ M.Kopal,⁵⁰ V.Koutsenko,^{15,30} M.Kräber,⁵³ H.H.Kuang,⁷ R.W.Kraemer,³⁸ A.Krüger,⁵² J.Kuijpers,³³ A.Kunin,¹⁵ P.Ladron de Guevara,²⁷ I.Laktineh,²⁶ G.Landi,¹⁹ M.Lebeau,²⁰ A.Lebedev,¹⁵ P.Lebrun,²⁶ P.Lecomte,⁵³ P.Lecoq,²⁰ P.Le Coultre,^{53,⊕} J.M.Le Goff,²⁰ Y.Lei,⁷ H.Leich,⁵² R.Leiste,⁵² M.Levtchenko,²⁹ P.Levtchenko,³⁷ C.Li,²⁴ L.Li,⁷ Z.C.Li,⁷ S.Likhoded,⁵² C.H.Lin,⁴⁸ W.T.Lin,⁴⁸ F.L.Linde,² L.Lista,³¹ Z.A.Liu,⁷ W.Lohmann,⁵² E.Longo,⁴² Y.S.Lu,⁷ C.Luci,⁴² L.Luminari,⁴² W.Lusteremann,⁵³ W.G.Ma,²⁴ X.H.Ma,⁷ Y.Q.Ma,⁷ L.Malgeri,²⁰ A.Malinin,³⁰ C.Maña,²⁷ J.Mans,⁴⁰ J.P.Martin,²⁶ F.Marzano,⁴² K.Mazumdar,¹¹ R.R.McNeil,⁶ S.Mele,^{20,31} X.W.Meng,⁷ L.Merola,³¹ M.Meschini,¹⁹ W.J.Metzger,³³ A.Mihul,¹³ A.van Mil,³³ H.Milcent,²⁰ G.Mirabelli,⁴² G.B.Mohanty,¹¹ B.Monteleoni,^{19,†} G.S.Muanza,²⁶ A.J.M.Muijs,² M.Musy,⁴² S.Nagy,¹⁷ R.Nahnhauser,⁵² V.A.Naumov,^{19,⊙} S.Natale,²² M.Napolitano,³¹ F.Nessi-Tedaldi,⁵³ H.Newman,³⁵ A.Nisati,⁴² T.Novak,³³ H.Nowak,⁵² R.Ofierzynski,⁵³ G.Organtini,⁴² I.Pal,⁵⁰ C.Palomares,²⁷ P.Paolucci,³¹ R.Paramatti,⁴² J.-F.Parriaud,²⁶ G.Passaleva,¹⁹ S.Patricelli,³¹ T.Paul,¹² M.Pauluzzi,³⁶ C.Paus,¹⁵ F.Pauss,⁵³ M.Pedace,⁴² S.Pensotti,²⁹ D.Perret-Gallix,⁴ B.Petersen,³³ D.Piccolo,³¹ F.Pierella,¹⁰ M.Pieri,¹⁹ M.Pioppi,³⁶ P.A.Piroué,⁴⁰ E.Pistolesi,²⁹

V.Plyaskin,³⁰ M.Pohl,²² V.Pojidaev,¹⁹ J.Pothier,²⁰ D.Prokofiev,³⁷ C.R.Qing,⁸ G.Rahal-Callot,⁵³ M.A.Rahaman,¹¹ P.Raics,¹⁷ N.Raja,¹¹ R.Ramelli,⁵³ P.G.Rancoita,²⁹ R.Ranieri,¹⁹ A.Raspereza,⁵² K.C.Ravindran,¹¹ P.Razis,³² S.Rembeczki,²⁸ D.Ren,⁵³ M.Rescigno,⁴² S.Reucroft,¹² P.Rewiersma,^{2,†} S.Riemann,⁵² K.Riles,³ B.P.Roe,³ A.Rojkov,^{53,33,19} L.Romero,²⁷ A.Rosca,⁵² S.Rosier-Lees,⁴ S.Roth,¹ J.A.Rubio,²⁰ G.Ruggiero,¹⁹ H.Rykaczewski,⁵³ R.Saidi,⁹ A.Sakharov,⁵³ S.Saremi,⁶ S.Sarkar,⁴² J.Salicio,²⁰ E.Sanchez,²⁷ C.Schäfer,²⁰ V.Schegelsky,³⁷ V.Schmitt,⁹ B.Schoeneich,⁵² H.Schopper,²³ D.J.Schotanus,³³ C.Sciacca,³¹ L.Servoli,³⁶ C.Q.Shen,⁷ S.Shevchenko,³⁵ N.Shivarov,⁴⁶ V.Shoutko,¹⁵ E.Shumilov,³⁰ A.Shvorob,³⁵ D.Son,⁴⁷ C.Souga,²⁶ P.Spillantini,¹⁹ M.Steuer,¹⁵ D.P.Stickland,⁴⁰ B.Stoyanov,⁴⁶ A.Straessner,²² K.Sudhakar,¹¹ H.Sulanke,⁵² G.Sultanov,⁴⁶ L.Z.Sun,²⁴ H.Sutet,⁵³ J.D.Swain,¹² Z.Szillasi,^{28,¶} X.W.Tang,⁷ P.Tarjan,¹⁷ L.Tauscher,⁵ L.Taylor,¹² B.Tellili,²⁶ D.Teyssier,²⁶ C.Timmermans,³³ Samuel C.C.Ting,¹⁵ S.M.Ting,¹⁵ S.C.Tonwar,¹¹ J.Tóth,¹⁴ G.Trowitzsch,⁵² C.Tully,⁴⁰ K.L.Tung,⁷ J.Ulbricht,⁵³ M.Unger,⁵² E.Valente,⁴² H.Verkooyen,² R.T.Van de Walle,³³ R.Vasquez,⁵⁰ G.Vesztergombi,¹⁴ I.Vetlitsky,³⁰ G.Viertel,⁵³ M.Vivargent,⁴ S.Vlachos,⁵ I.Vodopianov,²⁸ H.Vogel,³⁸ H.Vogt,⁵² I.Vorobiev,^{38,30} A.A.Vorobyov,³⁷ M.Wadhwa,⁵ R.G.Wang,⁷ Q.Wang,³³ X.L.Wang,²⁴ X.W.Wang,⁷ Z.M.Wang,²⁴ M.Weber,²⁰ R.van Wijk,² T.A.M.Wijnen,³³ H.Wilkens,³³ S.Wynhoff,⁴⁰ L.Xia,³⁵ Y.P.Xu,⁵³ J.S.Xu,⁷ Z.Z.Xu,²⁴ J.Yamamoto,³ B.Z.Yang,²⁴ C.G.Yang,⁷ H.J.Yang,³ M.Yang,⁷ X.F.Yang,⁷ Z.G.Yao,^{53,7} S.C.Yeh,⁴⁹ Z.Q.Yu,⁷ An.Zalite,³⁷ Yu.Zalite,³⁷ C.Zhang,⁷ F.Zhang,⁷ J.Zhang,⁷ S.Zhang,⁷ Z.P.Zhang,²⁴ J.Zhao,²⁴ S.J.Zhou,⁷ G.Y.Zhu,⁷ R.Y.Zhu,³⁵ Q.Q.Zhu,⁷ H.L.Zhuang,⁷ A.Zichichi,^{10,20,21} B.Zimmermann,⁵³ M.Zöller,¹ A.N.M.Zwart.²

- 1 III. Physikalisches Institut, RWTH, D-52056 Aachen, Germany[§]
- 2 NIKHEF, and University of Amsterdam, NL-1009 DB Amsterdam, The Netherlands
- 3 University of Michigan, Ann Arbor, MI 48109, USA
- 4 LAPP, IN2P3-CNRS, BP 110, F-74941 Annecy-le-Vieux CEDEX, France
- 5 Institute of Physics, University of Basel, CH-4056 Basel, Switzerland
- 6 Louisiana State University, Baton Rouge, LA 70803, USA
- 7 Institute of High Energy Physics, IHEP, 100039 Beijing, China[△]
- 8 ITP, Academia Sinica, 100039 Beijing, China
- 9 Humboldt University, D-10115 Berlin, Germany.
- 10 University of Bologna and INFN-Sezione di Bologna, I-40126 Bologna, Italy
- 11 Tata Institute of Fundamental Research, Mumbai (Bombay) 400 005, India
- 12 Northeastern University, Boston, MA 02115, USA
- 13 Institute of Atomic Physics and University of Bucharest, R-76900 Bucharest, Romania
- 14 Central Research Institute for Physics of the Hungarian Academy of

- Sciences, H-1525 Budapest 114, Hungary[‡]
- 15 Massachusetts Institute of Technology, Cambridge, MA 02139, USA
- 16 Panjab University, Chandigarh 160 014, India
- 17 KLTE-ATOMKI, H-4010 Debrecen, Hungary[¶]
- 18 UCD School of Physics, University College Dublin, Belfield, Dublin 4, Ireland
- 19 University of Florence and INFN, Sezione di Firenze, I-50019 Sesto Fiorentino, Italy
- 20 European Laboratory for Particle Physics, CERN, CH-1211 Geneva 23, Switzerland
- 21 World Laboratory, FBLJA Project, CH-1211 Geneva 23, Switzerland
- 22 University of Geneva, CH-1211 Geneva 4, Switzerland
- 23 University of Hamburg, D-22761 Hamburg, Germany
- 24 Chinese University of Science and Technology, USTC, Hefei, Anhui 230 029, China[△]
- 25 University of Lausanne, CH-1015 Lausanne, Switzerland
- 26 Institut de Physique Nucléaire de Lyon, IN2P3-CNRS, Université Claude Bernard, F-69622 Villeurbanne, France
- 27 Centro de Investigaciones Energéticas, Medioambientales y Tecnológicas, CIEMAT, E-28040 Madrid, Spain^b
- 28 Florida Institute of Technology, Melbourne, FL 32901, USA
- 29 INFN-Sezione di Milano, I-20133 Milan, Italy
- 30 Institute of Theoretical and Experimental Physics, ITEP, Moscow, Russia
- 31 INFN-Sezione di Napoli and University of Naples, I-80125 Naples, Italy
- 32 Department of Physics, University of Cyprus, Nicosia, Cyprus
- 33 Radboud University and NIKHEF, NL-6525 ED Nijmegen, The Netherlands
- 34 Osaka City University, Osaka 558-8585, Japan
- 35 California Institute of Technology, Pasadena, CA 91125, USA
- 36 INFN-Sezione di Perugia and Università Degli Studi di Perugia, I-06100 Perugia, Italy
- 37 Nuclear Physics Institute, St. Petersburg, Russia
- 38 Carnegie Mellon University, Pittsburgh, PA 15213, USA
- 39 INFN-Sezione di Napoli and University of Potenza, I-85100 Potenza, Italy
- 40 Princeton University, Princeton, NJ 08544, USA
- 41 University of California, Riverside, CA 92521, USA
- 42 INFN-Sezione di Roma and University of Rome, “La Sapienza”, I-00185 Rome, Italy
- 43 University and INFN, Salerno, I-84100 Salerno, Italy

- 44 University of California, San Diego, CA 92093, USA
- 45 University of Santiago de Compostela, E-15706 Santiago, Spain
- 46 Bulgarian Academy of Sciences, Central Lab. of Mechatronics and Instrumentation, BU-1113 Sofia, Bulgaria
- 47 The Center for High Energy Physics, Kyungpook National University, 702-701 Taegu, Republic of Korea
- 48 National Central University, Chung-Li, Taiwan, China
- 49 Department of Physics, National Tsing Hua University, Taiwan, China
- 50 Purdue University, West Lafayette, IN 47907, USA
- 51 Paul Scherrer Institut, PSI, CH-5232 Villigen, Switzerland
- 52 DESY, D-15738 Zeuthen, Germany
- 53 Eidgenössische Technische Hochschule, ETH Zürich, CH-8093 Zürich, Switzerland
- § Supported by the German Bundesministerium für Bildung, Wissenschaft, Forschung und Technologie.
- ‡ Supported by the Hungarian OTKA fund under contract numbers T019181, F023259 and T037350.
- ¶ Also supported by the Hungarian OTKA fund under contract number T026178.
- ♭ Supported also by the Comisión Interministerial de Ciencia y Tecnología.
- ‡ Also supported by CONICET and Universidad Nacional de La Plata, CC 67, 1900 La Plata, Argentina.
- △ Supported by the National Natural Science Foundation of China.
- ⊙ On leave from the Moscow Physical Engineering Institute (MePhI).
- ◇ On leave from JINR, RU-141980 Dubna, Russia.
- † Deceased
- ⊕ Corresponding author, e-mail: *Pierre.Le.Coultre@cern.ch*